




ARTICLE

DOI: 10.1038/s42004-018-0071-6

OPEN

# A complex metal-organic framework catalyst for microwave-assisted radical polymerization

Ha L. Nguyen <sup>1,2</sup>, Thanh T. Vu<sup>1</sup>, Dinh-Khoi Nguyen<sup>3</sup>, Christopher A. Trickett<sup>4</sup>, Tan L.H. Doan <sup>1,3</sup>, Christian S. Diercks<sup>4</sup>, Viet Q. Nguyen<sup>5</sup> & Kyle E. Cordova <sup>2,4</sup>

Metal-organic frameworks (MOFs) have emerged as promising materials for use in practical applications of renewable energy, water harvesting, and catalytic transformation. Here we report the design of a highly porous MOF, termed MOF-907. Single crystal X-ray diffraction analysis, in combination with topological deconstruction, revealed a MOF based on trigonal prismatic secondary building units linked together by triangular and linear units to form a previously unseen net (**nha**) with minimal transitivity, which is rational for these constituent building units. The catalytic properties of MOF-907 for the microwave-assisted radical polymerization of methyl methacrylate were demonstrated. MOF-907 produced a poly methyl methacrylate product in a short reaction time (30 min) with high yield (98%), high molecular weight (20,680 g mol<sup>-1</sup>), and low polydispersity (1.23).

<sup>1</sup>Center for Innovative Materials and Architectures (INOMAR), Vietnam National University–Ho Chi Minh City (VNU–HCM), Ho Chi Minh City 721337, Vietnam. <sup>2</sup>Center for Research Excellence in Nanotechnology (CENT), King Fahd University of Petroleum and Minerals, Dhahran 31261, Saudi Arabia. <sup>3</sup>Faculty of Chemistry, University of Science, VNU–HCM, Ho Chi Minh City 721337, Vietnam. <sup>4</sup>Berkeley Global Science Institute, University of California–Berkeley, Berkeley, CA 94720, USA. <sup>5</sup>National Key Lab for Polymer and Composite, Bach Khoa University, VNU–HCM, Ho Chi Minh City 721337, Vietnam. Correspondence and requests for materials should be addressed to H.L.N. (email: [nlha@inomar.edu.vn](mailto:nlha@inomar.edu.vn))

It is a central premise of reticular chemistry that structures of the highest symmetry (i.e., minimal transitivity) are the most likely to result from linking simple, symmetric building units<sup>1–4</sup>. This notion holds true for metal-organic frameworks (MOFs)<sup>5</sup> whose structures are simple in that they contain one kind of multi-metallic unit and one kind of organic linker. However, the premise of minimal transitivity is not as widely observed for more complex MOFs whose compositions extend beyond binary building units<sup>6–10</sup>. This is because the ratios of linkers incorporated within such MOF structures and their respective length ratios must be a perfect match. Indeed, this becomes increasingly difficult to control when moving toward multiple building units. Given the desire to increase the complexity of MOFs (i.e., increase the number of building units)<sup>11</sup>, the following questions arise: Can the transitivity principle be effectively extended? If so, what are these structures and what are their properties? For the first two questions, we know that complex MOFs constructed from multiple building units rarely follow the minimal transitivity principle (MOF-205 is a notable exception).

In this contribution, we describe a complex ternary MOF system, termed MOF-907, which is constructed from trigonal prismatic  $\text{Fe}_3\text{O}(-\text{CO}_2)_6$  clusters with triangular 4,4',4''-benzene-1,3,5-triyl-tris(benzoic acid) ( $\text{H}_3\text{BTB}$ ) and linear 2,6-naphthalenedicarboxylic acid ( $\text{H}_2\text{NDC}$ ) linkers. For this system, the ideal linker length ratio and linker incorporation is met for achieving a minimal transitive **nha** net. In addressing the third question, we elucidate the relationship between high symmetry and the favorable geometry of the pore structure within such systems, leading to this material's enhanced catalytic properties.

## Results

**Single crystal X-ray diffraction studies.** Single crystals of MOF-907 (Fig. 1 and Supplementary Figs. 1 and 2) were obtained upon heating a reaction mixture containing  $\text{H}_3\text{BTB}$ ,  $\text{H}_2\text{NDC}$ , and  $\text{Fe}(\text{NO}_3)_3 \cdot 9\text{H}_2\text{O}$  in *N,N*-dimethylformamide (DMF) at 120 °C for 24 h. Acetic acid, acting as a modulator to adjust the acidity, was also added to the reaction mixture (Supplementary Methods). Single crystal X-ray diffraction analysis revealed that MOF-907 crystallized in the body-centered cubic space group, *Im-3m* (No. 229), with a lattice parameter of  $a = 44.4781(14)$  Å (Supplementary Data 1 and Supplementary Table 1).

The structure of MOF-907 is made up of four hierarchical levels. These levels can be reduced down to the assembly of a primary cage comprised of six trigonal prismatic  $\text{Fe}_3\text{O}(-\text{CO}_2)_6$  clusters acting as vertices to form a distorted octahedral-shaped cage with a 12 Å diameter (Fig. 2a). In this primary cage, two tritopic  $\text{BTB}^{3-}$  linkers connect the vertices along opposing equatorial edges with the remaining coordination occurring across the faces to both of the axial vertices. Completing the primary cage are six  $\text{NDC}^{2-}$  linkers, two of which fill in the remaining equatorial edges and the other four connecting the equatorial vertices with those of the axial sites (on opposing axial edges from the  $\text{BTB}^{3-}$  axial face). These primary cages then assemble into the second level of the structure, in which each trigonal prismatic vertex of the primary octahedral cage is shared with another primary octahedral cage (Fig. 2a). The second level is created upon assembling eight primary cages into a cuboctahedral-shaped cage with a diameter of 19 Å (cuboctahedral cage 1, Fig. 2a). This gives rise to a square window with a diameter of ~13 Å. A third level is then built up from six cuboctahedral cage 1 units of 19 Å in diameter (cuboctahedral cage 2, Fig. 2a). Finally, the overall structure is realized through combining all three levels: one cuboctahedral cage 2, six cuboctahedral cage 1, and 24 total primary cages generating two types of 1-D interconnected pore channels due to the cubic lattice structure.

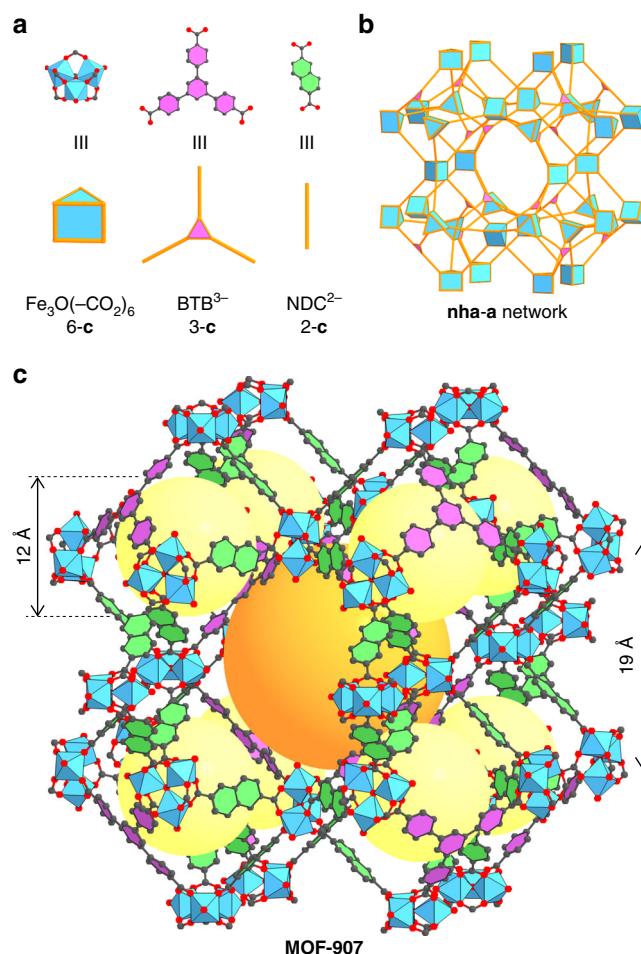


**Fig. 1** Structural representation of MOF-907. **(a, b)** Trigonal prismatic  $\text{Fe}_3\text{O}(-\text{CO}_2)_6$  clusters linked together by triangular 4,4',4''-benzene-1,3,5-triyl-tris(benzoate) ( $\text{BTB}^{3-}$ ) and linear 2,6-naphthalenedicarboxylate ( $\text{NDC}^{2-}$ ) linkers, corresponding to 6-connected, 3-connected, and 2-connected (-c) points of extension, respectively, yield a MOF with a previously unseen net, **nha** (depicted in augmented (-a) form). **(c)** The single crystal structure of MOF-907 is presented. Atom colors: Fe: blue polyhedra. C: black, and O: red. All H atoms are omitted for clarity. The yellow and orange spheres indicate the free space in the cages

**Topological analysis of MOF-907.** Topological deconstruction of MOF-907 was performed using ToposPro software<sup>12</sup>. For topological analysis, the  $\text{Fe}_3\text{O}(-\text{CO}_2)_6$  secondary building unit (SBU) and  $\text{BTB}^{3-}$  and  $\text{NDC}^{2-}$  linkers were first reduced into simplified nodes, resulting in 6-connected and 3-connected points of extension for  $\text{Fe}_3\text{O}(-\text{CO}_2)_6$  and  $\text{BTB}^{3-}$ , respectively. It is noted that NDC was represented as an edge when connecting the 6-c point of extension for the  $\text{Fe}_3\text{O}(-\text{CO}_2)_6$  nodes. Through this deconstruction, we uncovered the first case of a net, termed **nha**, with minimal transitivity based on trigonal prismatic SBUs linked together by triangular and linear units (Supplementary Fig. 3). Furthermore, this is only the second complex MOF structure, constructed from mixed linkers, to have adopted a minimal transitive net<sup>7</sup>. The transitivity of the **nha** tiling (face-to-face packing of cages) is described in terms of *pqrs* (where *p* is the number of vertices, *q* is the number of edges, *r* is the number of faces, and *s* is the type of tiles). For **nha**,  $pqrs = 2244$ . Further analysis of the tiling reveals three cages described as  $4[4^6] + 8[6] + 9[4^4.8^2]$ , respectively (where the symbol  $[...m^n...]$  denotes that there are *n* faces with *m*-membered rings) (Fig. 2b).

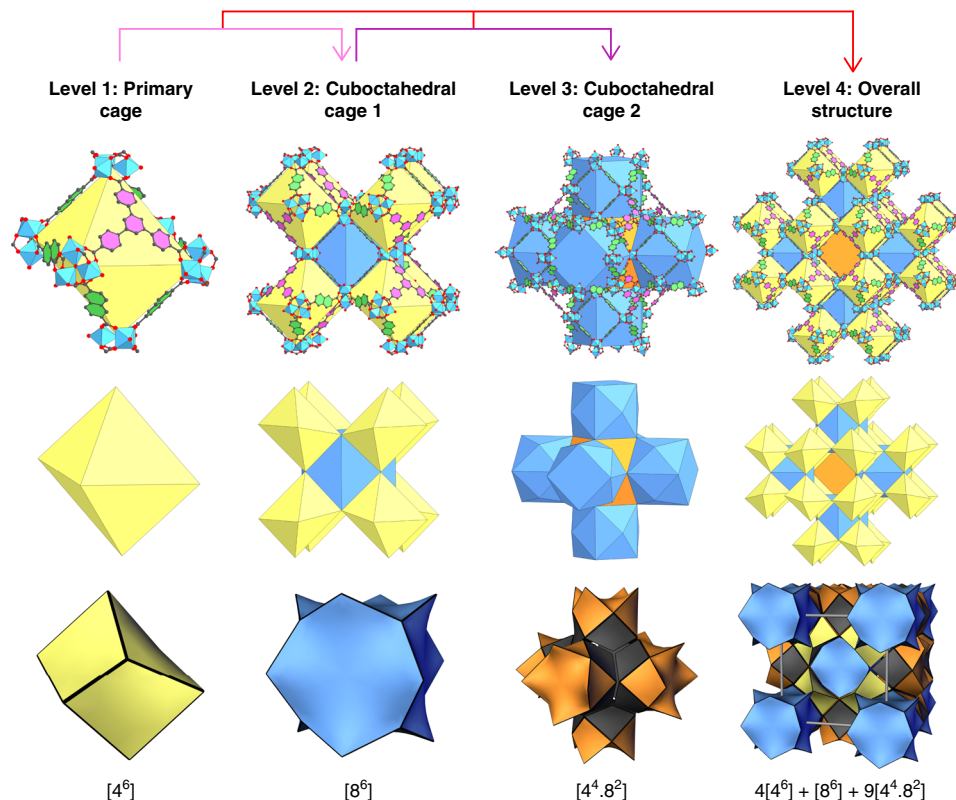


**Fig. 2** Conceptual basis for the realization of MOF-907 adopting the minimal transitive **nha** net. This structure is built up from four hierarchical levels. **a** At the fundamental level, a primary distorted octahedral cage consisting of six  $\text{Fe}_3\text{O}(\text{CO}_2)_6$  clusters connected by two  $\text{BTB}^{3-}$  and six  $\text{NDC}^{2-}$  linkers, is formed. A cuboctahedral cage 1 then assembles from eight vertex-sharing primary cages. This leads to the assembly of six of these cuboctahedral cages to form another cuboctahedral cage (cage 2). The overall structure then assembles through a combination of one cuboctahedral cage 2, six cuboctahedral cage 1, and 24 total primary cages. **b** The natural tiling of the **nha** topology is shown for each of the cages. Atom colors: Fe: blue polyhedral, C: black, and O: red.  $\text{BTB}^{3-}$  linkers are shown in filled pink to aid in distinguishing them from the  $\text{NDC}^{2-}$  linkers (filled green). H atoms are omitted for clarity

When considering the reason for realizing the **nha** net, it was evident that the ratio of the tritopic:ditopic linker lengths ( $L_T:L_D$ ; where  $L_T$  = length of the tritopic linker and  $L_D$  = length of the ditopic linker) played a critical role. Minimal transitive nets are achieved with the highest frequency for MOFs constructed with only one linker because they are the most symmetric. However, for the case of MOFs constructed from two (or more) linkers, the relative ratio of linker lengths must be a perfect fit to achieve maximal symmetry. Based on crystal structure evaluation and analyses, we observed that the ratio of linker lengths for MOF-907 ( $L_T:L_D = 0.90$ ) achieves this in contrast to other MOFs with similar constituent building units: MIL-142A ( $L_T:L_D = 1.29$ ), PCN-280 ( $L_T:L_D = 0.71$ ), and PCN-285 ( $L_T:L_D = 0.59$ ) (Fig. 3a and Supplementary Fig. 4). Upon further investigation into the reasoning behind MOF-907 adopting a minimal transitive net, we identified a second structural phenomenon: the ratio of the tritopic:ditopic linkers ( $N_T:N_D$ ; where  $N_T$  = the number of tritopic linkers and  $N_D$  = the number of ditopic linkers) connected to the  $\text{Fe}_3\text{O}$  SBU was variable. In fact, we found that there were three possible ratios when considering this structural phenomenon in Fe-based MOFs with the same constituent building units: (i) 4 tritopic and 2 ditopic linkers ( $N_T:N_D = 2$ ; ex. PCN-285, PCN-280, and MIL-142A-E); (ii) 3 tritopic and 3 ditopic linkers ( $N_T:N_D = 1$ ); and (iii) 2 tritopic and 4 ditopic linkers ( $N_T:N_D = 0.5$ ; ex. MOF-907) (Fig. 3). As such, we found that MOF-907 had perfectly-sized tritopic and ditopic linkers ( $L_T:L_D = 0.90$ ) and combination thereof incorporated within the SBU ( $N_T:N_D = 0.5$ ), which led to the realization of the highest symmetry minimal transitive network for MOFs comprised of

these building units (Fig. 3). It is noted that an optimal input ratio of starting materials (molar ratio of  $\text{BTB}:\text{NDC} = 0.5\text{--}0.75$ ) together with an exact amount of modulator (AcOH, 0.2 mL) were required to produce the resulting structure during crystal formation.

After solvent-exchange and full activation, the activated sample was measured powder X-ray diffraction (PXRD) which is in agreement with the as-synthesized and simulated pattern (Supplementary Fig. 5). The formulation of the chemical structure was achieved through a combination of digested  $^1\text{H}$  nuclear magnetic resonance spectroscopy (NMR), elemental microanalysis (EA), thermal gravimetric analysis (TGA), Mössbauer spectroscopy, and Fourier transform infrared spectroscopy (FT-IR) measurements (Supplementary Figs. 6–8). The digested  $^1\text{H}$  NMR spectrum confirmed the ratio of  $\text{BTB}:\text{NDC}$  to be 1:3 (Supplementary Fig. 11). Following this, EA was employed to resolve MOF-907's chemical formula as  $\text{Fe}^{\text{III}}_3\text{O}(\text{OH})(\text{BTB})_{0.67}(\text{NDC})_2$ . TGA was then utilized to provide further support for this formulation. After heating activated MOF-907 in air up to 600 °C, the observed residual mass (22.3%) was consistent with the expected mass of  $\text{Fe}_2\text{O}_3$  (23.4%) after framework decomposition. The presence of one capping  $\text{OH}^-$  ligand (necessary for charge balancing) was proven by FT-IR, where an O-H stretching frequency vibration at 520  $\text{cm}^{-1}$  was clearly observed (Supplementary Fig. 7)<sup>13, 14</sup>. To ensure the oxidation state of Fe in MOF-907 was correct, Mössbauer spectroscopy was employed to confirm the presence of only  $\text{Fe}^{\text{III}}$  within the structure (Supplementary Fig. 8). Finally, the permanent porosity of MOF-907 was proven by  $\text{N}_2$  adsorption

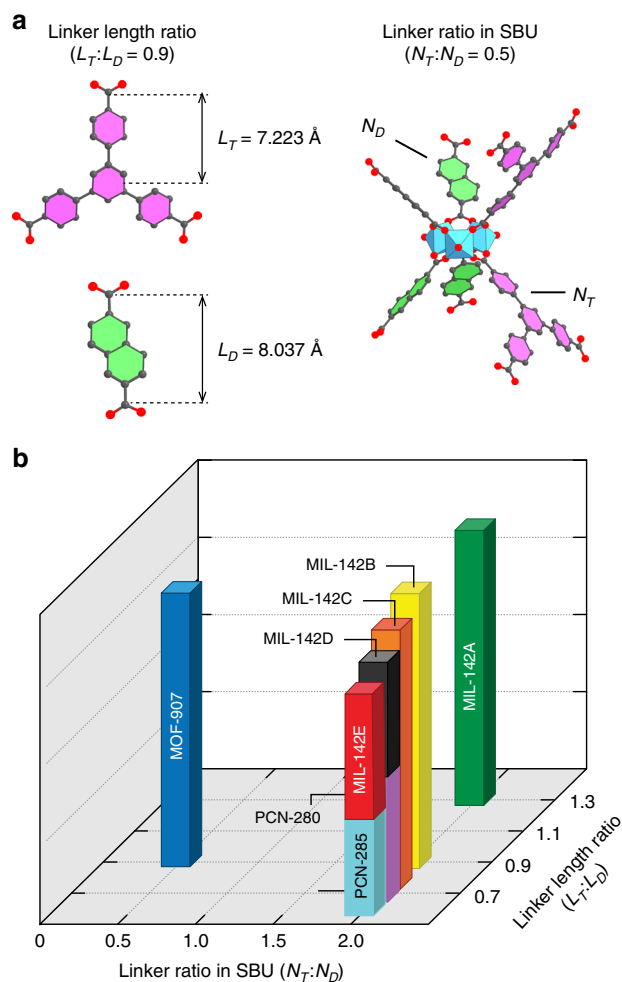


**Fig. 3** Principles for achieving minimal transitivity in MOF-907. **a** Two structural features played pivotal roles in producing MOF-907, which adopts a highly symmetric, minimal transitive net: The ratio of tritopic: ditopic linker lengths ( $L_T:L_D$ ); and the proportion of tritopic to ditopic linker incorporated within the SBU ( $N_T:N_D$ ). **b** These structural features are guiding principles for achieving the highest symmetric material based on  $\text{Fe}_3\text{O}$  SBUs and mixed tritopic and ditopic linkers

isotherms at 77 K. MOF-907 exhibited a Brunauer–Emmett–Teller (Langmuir) surface area of 1600 (1800)  $\text{m}^2\text{g}^{-1}$  (Supplementary Figs. 9 and 10), which is slightly less than the theoretical geometrical surface area determined from the crystal structure (2000  $\text{m}^2\text{g}^{-1}$ ).

**Catalytic properties of MOF-907.** Motivated by the high porosity and appropriately-sized 1-D interconnected pore channels of MOF-907 in conjunction with the presence of strong Lewis acidity via potential coordinatively unsaturated metal sites in the  $\text{Fe}_3\text{O}$  SBUs<sup>15–17</sup>, we sought to assess whether such a structure would have, as a natural outcome, a high performance for catalytic applications. As such, MOF-907 was employed as a catalyst for the microwave-assisted radical polymerization of methyl methacrylate (MMA; Fig. 4)–a model reaction that requires a catalyst with strong Lewis acidity<sup>18,19</sup>. Initial attention was placed on optimizing the catalysis conditions, including the amount of MOF-907 catalyst, co-initiator, organic solvent, and reaction time. As such, two different co-initiators, ethyl  $\alpha$ -bromophenylacetate (EBPA) and ethyl  $\alpha$ -bromoisobutyrate (EBiB), were tested (Supplementary Fig. 12). For the reactions

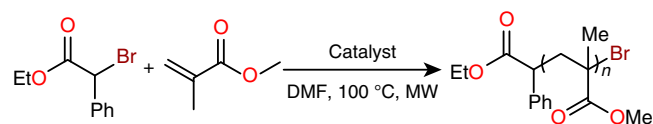


**Fig. 4** Polymerization reaction. General polymerization reaction of MMA

**Table 1** Microwave-assisted radical polymerization of methyl methacrylate

Entry <sup>a</sup>	Catalyst [mol%]	Yield [%]	$M_n$ [ $\text{g mol}^{-1}$ ]	$M_w/M_n$
MOF-907 <sup>b</sup>	0.06	98	20,680	1.23
Ni-VNU-74 (II) <sup>b</sup>	0.06	10	12,300	1.45
HKUST-1 <sup>b</sup>	0.06	43	11,060	1.44
MIL-101(Fe) <sup>b</sup>	0.06	20	15,080	1.35
PCN-280 <sup>b</sup>	0.06	35	13,860	1.32
PCN-285 <sup>b</sup>	0.06	45	17,100	1.41
$\text{FeCl}_3$ <sup>b,c</sup>	0.06	12	8,000	1.62
MOF-907 <sup>d</sup>	0.06	43	14,230	1.43
MOF-907 <sup>a,e</sup>	0.06	68	15,550	1.31
MOF-907 <sup>f</sup>	0.06	n.d.	n.a.	n.a.
MOF-907 <sup>g</sup>	0	n.d.	n.a.	n.a.

<sup>a</sup>Reaction conditions: MMA (2.8 M in DMF), catalyst (0.06 mol% compared to MMA), initiator: EBPA or EBiB (0.45 mol%) at 100 °C, 30 min and 200 W

<sup>b</sup>Reaction conditions: MMA (5.6 M in DMF), catalyst (0.06 mol% compared to MMA mol), initiator (EBiB, 0.45 mol%) at 100 °C, 30 min and 200 W

<sup>c</sup>Homogeneous catalytic performance

<sup>d</sup>Using EBPA as initiator

<sup>e</sup>Using EBiB as initiator

<sup>f</sup>The reaction was performed in the absence of microwave irradiation

<sup>g</sup>The reaction was performed without MOF-907

using EBiB, polyMMA was produced in a yield of 68% using MOF-907 catalyst (0.06 mol% loading), with an average  $M_n = 15,550\text{ g mol}^{-1}$  and a polydispersity index (PDI) of 1.31. When EBPA was used as the co-initiator, polyMMA formed in lower yield (43%) and with an overall lower  $M_n$  (14,230  $\text{g mol}^{-1}$ ) and higher PDI (1.43) (Table 1 and Supplementary Table 2 and Supplementary Fig. 13).

Control experiments in which the MOF-907 catalyst or microwave irradiation was absent demonstrated no observable product formation. Without microwave irradiation, radical generation and propagation cannot occur, which would prohibit the polymerization process. The effect of monomer concentration on the quality of product was subsequently investigated by reducing the amount of solvent used in the reaction. Specifically, halving the amount of DMF added to the mixture, in effect, doubled the monomer concentration, increased the  $M_n$  value from 15,550 to 20,680  $\text{g mol}^{-1}$ , and lowered the PDI to 1.23 with a nearly quantitative yield of 98% (Table 1 and Supplementary Table 3).

In order to ensure that the catalytic activity was derived from the Lewis acidic SBUs in MOF-907, we employed other MOF catalysts, specifically Ni-VNU-74(II)<sup>20</sup> and HKUST-1<sup>21</sup>, which contain SBUs with open Lewis acidic active sites. As expected, both Ni-VNU-74(II) and HKUST-1 were active; however, MOF-907 outperformed both of these materials under identical reaction conditions in producing high  $M_n$  polyMMA product, in higher yields, and with a lower PDI (Table 1). This is attributed to the strong Lewis acidic sites of Fe-based MOFs as compared to Ni-based or Cu-based MOFs<sup>15–17</sup>. Additionally, the pore size of MOF-907 is more suitable for the polymerization reaction than those of Ni-VNU-74(II) (23.6 Å 1-D mesopores) and HKUST-1 (8 Å 3-D arrangement pores). It is noted that the MIL-142 series

would be ideal comparative catalysts due to their identical building unit composition,<sup>8</sup> however, after exhaustive attempts, we were unable to reproduce these materials experimentally (Note: no crystallographic information files were reported or found in the Cambridge Crystallographic Data Center (CCDC) for this series). Our attention then turned to comparing the performance of MOF-907 with PCN-280<sup>9</sup> and MIL-101(Fe)<sup>22</sup>—both of which are constructed from the same Fe<sub>3</sub>O SBU active site.

As shown in Table 1, polyMMA products with much lower  $M_n$  (15,080 and 13,860 g mol<sup>-1</sup>) and higher PDI (1.35 and 1.32) values were obtained when using MIL-101(Fe) and PCN-280, respectively. Furthermore, MOF-907 outperformed these catalysts in terms of yield (98% v. 20% and 35% for MOF-907 v. MIL-101(Fe) and PCN-280, respectively). Since identical molar amounts of catalyst were used, the number of Fe<sup>III</sup> active sites in MOF-907 is equal to MIL-101(Fe) and PCN-280<sup>23, 24</sup>. Hence, we concluded that structural features, imparted by the topological network of MOF-907, played a pivotal role in enhancing the catalytic performance. Specifically, the monomers (substrates) have to be well-distributed throughout the pores in order to fully interact with the Fe<sub>3</sub>O SBUs. If this occurs, then one can take full advantage of the intrinsic catalytic active sites of the MOF material<sup>25</sup>. Indeed, MOF-907 possesses 1-D interconnected channels, 19 Å in size, with an accessible pore window of 13 Å. These appropriately-sized 1-D channels are better suited to disperse the substrates for polymerization than the small 3-D pore windows found in PCN-280 (12 Å) and MIL-101(Fe) (14 Å).

The scanning electron microscope (SEM) image of bulk phase (large-scale synthesis) of MOF-907 was also measured to confirm the phase purity and uniformity of the sample (Supplementary Fig. 14). To ensure that the catalysis is in fact taking place within the internal pore environment as opposed to the external surface, we then carried out control experiments using MOF-907 crystals of varying size. The yield of polyMMA experienced little change when using 29 μm-sized MOF-907 particles (98% yield) or 92 μm-sized MOF-907 particles (91% yield) (Supplementary Fig. 15). This is an important control experiment as smaller-sized crystals typically offer higher catalytic activity if the catalysis is taking place on the external surface<sup>26</sup>. Since there was little change in polyMMA yield when using different sized particles of MOF-907, it is effectively concluded that the reaction took place mostly within the pores as a result of the unique structural features of MOF-907<sup>26</sup>. It is noted that for the comparative studies, as shown in Table 1, the particle sizes of MIL-101(Fe) (6 μm), HKUST-1 (18 μm), PCN-280 (37 μm), and Ni-VNU-74(II) (28 μm) were all relatively smaller than the particle size of MOF-907 (Supplementary Fig. 16). This confirms that the structural features of MOF-907 are the most important factor for achieving exceptional catalytic performance.

In order to validate the effect of the catalyst's pore size on the polymerization reaction, mesoporous PCN-285 (22 Å)<sup>9</sup>, constructed from BTB and 4,4'-azoBDC linkers, was employed as a catalyst in the polymerization of MMA. The molecular weight of polyMMA produced by PCN-285 (17,100 g mol<sup>-1</sup>) was smaller than that of the MMA polymer produced by MOF-907 (20,680 g mol<sup>-1</sup>). The PDI value of polyMMA, obtained by MOF-907, was also lower than PCN-285 (1.23 compared to 1.41, respectively). The catalytic activity of MOF-907 was further investigated by carrying out the polymerization reaction using a larger-sized monomer, benzyl methacrylate (BMA) (Supplementary Methods). Under identical conditions to those used in the polyMMA synthesis, polyBMA product was achieved with a relatively high  $M_n$  (14,100 g mol<sup>-1</sup>), high yield (76%), and low PDI (1.59) when using EBPA as the initiator (Supplementary Fig. 17). MOF-907 again outperforms comparative catalysts for this reaction (Supplementary Table 4 and 5).

## Discussion

While conventional<sup>27, 28</sup> and photocatalyzed radical polymerization<sup>26, 29–31</sup> is performed over one day, the microwave-assisted polymerization of MMA by MOF-907 was achieved in just 30 min (Table 1)<sup>26–34</sup>. A detailed kinetic study of this process was performed by monitoring the decrease in MMA concentration as a function of reaction time. Consequentially, the polymerization was a zero-order reaction, thus exhibiting independence from the reaction rate and concentration of MMA (Supplementary Fig. 18). MOF-907 also offers the advantage of recyclability. Over the course of three consecutive reactions, the crystallinity and structural integrity remained intact as evidenced by powder X-ray diffraction analysis (Supplementary Fig. 19). The turnover number was found to be 493 with no noticeable loss in catalytic activity observed as indicated by GPC and NMR analysis (Supplementary Figs. 20–22 and Supplementary Tables 6 and 7). Given the performance of MOF-907, it is likely that the strong Lewis acidic sites, derived from the Fe<sub>3</sub>O SBUs<sup>15–17</sup>, contributed to fast activation and stabilization of free radicals and, thus, induced chain-growth propagation<sup>35–40</sup>. Indeed, these factors were critical in producing monodisperse, high molecular weight polyMMA.

## Methods

**Synthesis and characterization of MOF-907.** H<sub>3</sub>BTB (0.012 g, 0.027 mmol) and H<sub>2</sub>NDC (0.01 g, 0.046 mmol) were dissolved in 3 mL DMF. A mixture of 1 mL DMF and acetic acid (0.20 mL, 3.49 mmol) containing iron(III) nitrate nonahydrate (0.02 g, 0.050 mmol) was then added to the solution containing H<sub>3</sub>BTB and H<sub>2</sub>NDC. The reacted solution was subsequently placed in a glass 8 mL vial and heated at 120 °C for 24 h. After that time elapsed, orange cube-shaped crystals were then collected by decantation.

**Large-scale synthesis of MOF-907.** H<sub>3</sub>BTB (0.36 g, 0.81 mmol) and H<sub>2</sub>NDC (0.30 g, 1.38 mmol) were dissolved in 90 mL of DMF. A mixture of 30 mL DMF and acetic acid (6.0 mL, 104.7 mmol) containing iron(III) nitrate nonahydrate (0.60 g, 1.5 mmol) was then added to the solution H<sub>3</sub>BTB and H<sub>2</sub>NDC. The reacted solution was subsequently placed in a 200 mL glass bottle and heated at 120 °C for 24 h. The orange powder was cooled down to room temperature and collected by decantation. The product was then washed with DMF (3 × 60 mL, each day) to remove the starting reagents. MOF-907 was immersed in anhydrous acetone for 3 days (3 × 60 mL, each day). A 100 mg activated sample (21% yield based on iron(III) nitrate nonahydrate) was collected after evacuating at 90 °C for 24 h. EA of activated sample: Calcd. for C<sub>42</sub>H<sub>23</sub>O<sub>17</sub>Fe<sub>3</sub>·0.75C<sub>3</sub>H<sub>7</sub>NO (C<sub>3</sub>H<sub>7</sub>NO = DMF) = Fe<sup>III</sup><sub>3</sub>O(OH)(BTB)<sub>2/3</sub>(NDC)<sub>2</sub>·0.75DMF: C, 52.00; H, 2.79; N, 1.03%. Found: C, 54.16; H, 3.32; N, 0.96%. Noted: DMF is the guest molecules inside the pores. Characterization details are presented in the Supplementary Methods.

**Single crystal X-ray diffraction studies.** Data was collected at beamline 11.3.1 at the Advanced Light Source, Lawrence Berkeley National Lab at 0.77490 Å. A single crystal of MOF-907 was isolated from the mother liquor of the reaction, mounted on a MiTeGen® kapton loop and placed in a 100(2) K nitrogen cold stream.

The data was processed with the Bruker APEX2 software package, integrated using SAINT v8.37 A and corrected for absorption by SADABS 2016/2 routines (no correction was made for extinction or decay). The structures were solved by intrinsic phasing (SHELXT 2014/4) and refined by full-matrix least squares on F<sup>2</sup> (SHELXL-2014-7). Once the framework atoms were located in the difference Fourier maps, the SQUEEZE routine in PLATON was performed to remove scattering from disordered guest molecules residing in the pores. The details of the single crystal refinement are found in the Supplementary Table 1.

**Polymerization of methyl methacrylate.** A 3.0 mg of activated MOF-907 (0.0032 mmol) was loaded into a 10 mL glass vial for use in the microwave system. 1.0 mL of DMF (13 mmol), 301 μL of methyl methacrylate (MMA, 2.81 mmol), and 1.9 μL of ethyl α-bromoisobutyrate (EBiB, 1.29 × 10<sup>-5</sup> mmol) or 2.3 μL ethyl α-bromophenylacetate (EBPA, 1.29 × 10<sup>-5</sup> mmol) were then added into the vial. The vial was sealed with a microwave cap. The reaction system was stirred for 30 min at room temperature (covered with Al foil to prevent light interference) before loading into the microwave system. The synthesis condition for the polymerization reaction was set up at 100 °C and 30 min with 200 W of power under a closed system. When the reaction was completed, MOF-907 was collected by centrifugation and washed with dichloromethane 3–5 times. The polyMMA product was crystallized in a solution of 30 mL MeOH and washed with methanol 3 times. The polymer was dried at room temperature for 2 days or under vacuum for 2 h. The following conditions were optimized: amount of initiator, different

concentration of the reaction, temperature, power, and the reaction time. The reported conditions above are optimized. The same procedure was applied using other catalysts (HKUST-1, Ni-VNU-74(II), and FeCl<sub>3</sub>).

### Data availability

Crystallographic data for MOF-907 was deposited in the CCDC. The deposition number is 1547518. This data can be obtained free of charge from the Cambridge Crystallographic Data Centre via [www.ccdc.cam.ac.uk/data\\_request/cif](http://www.ccdc.cam.ac.uk/data_request/cif). All other data that support the findings in this study are available from the corresponding author upon reasonable request.

Received: 8 June 2018 Accepted: 12 September 2018

Published online: 23 October 2018

### References

1. Furukawa, H., Cordova, K. E., O’Keeffe, M. & Yaghi, O. M. The chemistry and applications of metal-organic frameworks. *Science* **341**, 1230444 (2013).
2. Cordova, K. E. & Yaghi, O. M. The ‘folklore’ and reality of reticular chemistry. *Mater. Chem. Front.* **1**, 1304–1309 (2017).
3. Hoffmann, F. & Fröba, M. Network topology In: *The Chemistry of Metal-Organic Frameworks* (ed. Kaskel, S.) 5–40 (Wiley-VCH Verlag GmbH & Co. KGaA, Weinheim, 2016).
4. Li, M., Li, D., O’Keeffe, M. & Yaghi, O. M. Topological analysis of metal-organic frameworks with polytopic linkers and/or multiple building units and the minimal transitivity principle. *Chem. Rev.* **114**, 675–702 (2014).
5. Ren, G. J. et al. Construction of a polyhedron decorated MOF with a unique network through the combination of two classic secondary building units. *Chem. Commun.* **52**, 2079–2082 (2016).
6. Furukawa, H., Muller, U. & Yaghi, O. M. “Heterogeneity within order” in metal-organic frameworks. *Angew. Chem. Int. Ed.* **54**, 3417–3430 (2015).
7. Furukawa, H. et al. Ultrahigh porosity in metal-organic frameworks. *Science* **239**, 424–428 (2010).
8. Chevreau, H. et al. Mixed-linker hybrid superpolyhedra for the production of a series of large-pore Iron(III) carboxylate metal-organic frameworks. *Angew. Chem. Int. Ed.* **52**, 5056–5060 (2013).
9. Feng, D. et al. Kinetically tuned dimensional augmentation as a versatile synthetic route towards robust metal-organic frameworks. *Nat. Commun.* **5**, 5723 (2014).
10. Koh, K., Wong-Foy, A. G. & Matzger, A. J. A porous coordination copolymer with over 5000 m<sup>2</sup>/g BET surface area. *J. Am. Chem. Soc.* **132**, 15005–15010 (2010).
11. Chen, Q. et al. A controllable gate effect in cobalt (II) organic frameworks by reversible structure transformations. *Angew. Chem. Int. Ed.* **52**, 11550–11553 (2013).
12. Blatov, V. A., Shevchenko, A. P. & Proserpio, D. M. Applied topological analysis of crystal structures with the program package ToposPro. *Cryst. Growth Des.* **14**, 3576–3586 (2014).
13. Davidson, G. in *Spectroscopic Properties of Inorganic and Organometallic Compounds*. (ed. Greenwood, N. N.) 377–520 (Royal Society of Chemistry, United Kingdom, 2007).
14. Peng, L. et al. Using predefined M<sub>3</sub>(μ<sub>3</sub>-O) clusters as building blocks for an isostructural series of metal-organic frameworks. *ACS Appl. Mater. Interf.* **9**, 23957–23966 (2017).
15. Liu, T. F. et al. Topology-guided design and syntheses of highly stable mesoporous porphyrinic zirconium metal-organic frameworks with high surface area. *J. Am. Chem. Soc.* **137**, 413–419 (2015).
16. Xiao, D. J., Oktawiec, J., Milner, P. J. & Long, J. R. Pore environment effects on catalytic cyclohexane oxidation in expanded Fe<sub>2</sub>(dobdc) analogues. *J. Am. Chem. Soc.* **138**, 14371–14379 (2016).
17. Hu, Z. & Zhao, D. Metal-organic frameworks with Lewis acidity: synthesis, characterization, and catalytic applications. *CrystEngComm* **19**, 4066–4081 (2017).
18. Isobe, Y., Fujioka, D., Habaue, S. & Okamoto, Y. Efficient Lewis acid-catalyzed sterecontrolled radical polymerization of acrylamides. *J. Am. Chem. Soc.* **123**, 7180–7181 (2001).
19. Matsumoto, M. et al. Lewis-Acid-Catalyzed interfacial polymerization of covalent organic framework films. *Chem* **4**, 308–317 (2018).
20. Nguyen, B. T., Nguyen, H. L., Nguyen, T. C., Cordova, K. E. & Furukawa, H. High methanol uptake capacity in two new series of metal-organic frameworks: promising materials for adsorption-driven heat pump applications. *Chem. Mater.* **28**, 6243–6249 (2016).
21. Prestipino, C. et al. Local structure of framework Cu (II) in HKUST-1 metallorganic framework: spectroscopic characterization upon activation and interaction with adsorbates. *Chem. Mater.* **18**, 1337–1346 (2006).
22. Taylor-Pashow, K. M. L., Della Rocca, J., Xie, Z., Tran, S. & Lin, W. Postsynthetic modifications of iron-carboxylate nanoscale metal-organic frameworks for imaging and drug delivery. *J. Am. Chem. Soc.* **131**, 14261–14263 (2009).
23. Li, B., Chrzanowski, M., Zhang, Y. & Ma, S. Applications of metal-organic frameworks featuring multi-functional sites. *Coord. Chem. Rev.* **307**, 106–129 (2016).
24. Shui, J., Chen, C., Grabstanowicz, L., Zhao, D. & Liu, D. Highly efficient nonprecious metal catalyst prepared with metal-organic framework in a continuous carbon nanofibrous network. *Proc. Natl Acad. Sci.* **112**, 10629–10634 (2015).
25. Wang, F. et al. Active site dependent reaction mechanism over Ru/CeO<sub>2</sub> catalyst toward CO<sub>2</sub> methanation. *J. Am. Chem. Soc.* **138**, 6298–6305 (2016).
26. Nguyen, H. L. et al. A titanium-organic framework: engineering of the band-gap energy for photocatalytic property enhancement. *ACS Catal.* **7**, 338–342 (2017).
27. Hou, T., Zhang, P., Zhou, X., Cao, X. & Zhao, Y. Synthesis of well-defined polymers grafted onto fumed silica by chain exchange reaction and highly pure block copolymers thereby. *Chem. Commun.* **46**, 7397–7399 (2010).
28. Perro, A. & Manoharan, V. N. Bulk synthesis of polymer-inorganic colloidal clusters. *Langmuir* **26**, 18669–18675 (2010).
29. Nguyen, H. L. et al. A titanium-organic framework as an exemplar of combining the chemistry of metal- and covalent-organic frameworks. *J. Am. Chem. Soc.* **138**, 4330–4333 (2016).
30. Fors, B. P. & Hawker, C. J. Control of a living radical polymerization of methacrylates by light. *Angew. Chem. Int. Ed.* **51**, 8850–8853 (2012).
31. Chen, M., Zhong, M. & Johnson, J. A. Light-controlled radical polymerization: Mechanisms, methods, and applications. *Chem. Rev.* **116**, 10167–10211 (2016).
32. Cheng, Z., Zhu, X., Chen, M., Chen, J. & Zhang, L. Atom transfer radical polymerization of methyl methacrylate with low concentration of initiating system under microwave irradiation. *Polymer* **44**, 2243–2247 (2003).
33. Chen, X.-P. & Qiu, K.-Y. ‘Living’ radical polymerization of styrene with AIBN/FeCl<sub>3</sub>/PPh<sub>3</sub> initiating system via a reverse atom transfer radical polymerization process. *Polym. Int.* **49**, 1529–1533 (2000).
34. Bolm, C., Legros, J., Le Pailh, J. & Zani, L. Iron-catalyzed reactions in organic synthesis. *Chem. Rev.* **104**, 6217–6254 (2004).
35. Harding, J. L., Metz, J. M. & Reynolds, M. M. A tunable, stable, and bioactive MOF catalyst for generating a localized therapeutic from endogenous sources. *Adv. Funct. Mater.* **24**, 7503–7509 (2014).
36. Garibay, S. L., Wang, Z. & Cohen, S. M. Evaluation of heterogeneous metal-organic framework organocatalysts prepared by postsynthetic modification. *Inorg. Chem.* **49**, 8086–8091 (2010).
37. Kamigaito, M. Recent developments in metal-catalyzed living radical polymerization. *Polym. J.* **43**, 105–120 (2011).
38. Satoh, K., Ozawa, S., Mizutani, M., Nagai, K. & Kamigaito, M. Sequence-regulated vinyl copolymers by metal-catalysed step-growth radical polymerization. *Nat. Commun.* **1**, 6 (2010).
39. Fujimura, K., Ouchi, M. & Sawamoto, M. Ferrocene cocatalysis for iron-catalyzed living radical polymerization: active, robust, and sustainable system under concerted catalysis by two iron complexes. *Macromolecules* **48**, 4294–4300 (2015).
40. Dadashi-Silab, S., Pan, X. & Matyjaszewski, K. Photoinduced Iron-catalyzed atom transfer radical polymerization with ppm levels of iron catalyst under blue light irradiation. *Macromolecules* **50**, 7967–7977 (2017).

### Acknowledgements

H.L.N. acknowledges financial support from VNU-HCM (No. B2017-50-01). K.E.C. is grateful for collaborations with and support from S. Aramco (Project No. ORCP2390). We extend our gratitude to Prof. Davide M. Proserpio (University of Milan) and Prof. Michael O’Keeffe (Arizona State University) for advanced discussions on topological analysis. H.L.N. also acknowledges Dr. Hiroyasu Furukawa (UC Berkeley), Mr. Ahmed M. Alloush (KFUPM, Saudi Arabia), Mr. Duy-Khoi Nguyen, Mr. Dat N. X. Mai, Ms. Trang T. M. Nguyen (VNU-HCM), and Mr. Bao N. Truong (KITECH, Korea) for helpful discussions and assistance. We thank Prof. Christopher J. Chang (UC Berkeley) for the use of the Mössbauer spectrometer and Mr. Khetpakorn Chakarawet (UC Berkeley) for help with Mössbauer data collection and analysis.

### Author contributions

H.L.N., T.T.V., C.A.T., C.S.D. and T.L.H.D. were the contributors for designing the synthesis and performing structural characterization. H.L.N., D.-K.N., T.T.V. and V.Q.N.

carried out and analyzed the data for the catalytic studies. K.E.C. and H.L.N. contributed towards the design of the work, interpretation of the results, and editing of the manuscript.

### Additional information

**Supplementary information** accompanies this paper at <https://doi.org/10.1038/s42004-018-0071-6>.

**Competing interests:** The authors declare no competing interests.

**Reprints and permission** information is available online at <http://npg.nature.com/reprintsandpermissions/>

**Publisher's note:** Springer Nature remains neutral with regard to jurisdictional claims in published maps and institutional affiliations.



**Open Access** This article is licensed under a Creative Commons Attribution 4.0 International License, which permits use, sharing, adaptation, distribution and reproduction in any medium or format, as long as you give appropriate credit to the original author(s) and the source, provide a link to the Creative Commons license, and indicate if changes were made. The images or other third party material in this article are included in the article's Creative Commons license, unless indicated otherwise in a credit line to the material. If material is not included in the article's Creative Commons license and your intended use is not permitted by statutory regulation or exceeds the permitted use, you will need to obtain permission directly from the copyright holder. To view a copy of this license, visit <http://creativecommons.org/licenses/by/4.0/>.

© The Author(s) 2018